Postprint of: New Phytologist (2021) doi: 10.1111/nph.17577

Rapid report

Linking xylem network failure with leaf tissue death

Authors:

Timothy Brodribb[1*] ORCID iD- 0000-0002-4964-6107

Craig R. Brodersen[2*] ORCID iD- 0000-0002-0924-2570

Marc Carriqui[1] ORCID iD- 0000-0002-0153-2602

Vanessa Tonet[1] ORCID iD- 0000-0002-8373-5779

Celia Rodriguez Dominguez[3] ORCID iD- 0000-0003-2352-0829

Scott McAdam[4] ORCID iD- 0000-0002-9625-6750

Affiliations:

[1]School of Biological Sciences, University of Tasmania, Sandy Bay, Tasmania 7001, Australia

[2]School of the Environment, Yale University, New Haven, CT 06511, USA

[3] Irrigation and Crop Ecophysiology Group, Instituto de Recursos Naturales y Agrobiología de Sevilla (IRNAS, CSIC), Avda. Reina Mercedes, 10, 41012, Sevilla, Spain.

[4]Purdue Center for Plant Biology, Department of Botany and Plant Pathology, Purdue University, West Lafayette, Indiana 47907

*Correspondence to: timothyb@utas.edu.au and craig.brodersen@yale.edu

Received: 15 April 2021

Summary:

- Global warming is expected to dramatically accelerate forest mortality as temperature and drought intensity increase. Predicting the magnitude of this impact urgently requires an understanding of the process connecting atmospheric drying to plant tissue damage. Recent episodes of forest mortality worldwide have been widely attributed to dry conditions causing acute damage to plant vascular systems. Under this scenario vascular embolisms produced by water stress are thought to cause plant death, yet this hypothetical trajectory has never been empirically demonstrated.
- Here we provide foundational evidence connecting failure in the vascular network of leaves with tissue damage caused during water stress.
- We observe a catastrophic sequence initiated by water column breakage under tension in leaf veins which severs local leaf tissue water supply, immediately causing acute cellular dehydration and irreversible damage.
- By highlighting the primacy of vascular network failure in the death of leaves exposed to drought or evaporative stress our results provide a strong mechanistic foundation upon which models of plant damage in response to dehydration can be confidently structured.

Introduction

Photosynthesis and growth of vascular plants relies on the maintenance of an efficient vascular connection between water in the soil and leaves. Water moves passively in a pipeline of xylem tissue, following a tensile gradient from soil to leaves where it replaces water lost as transpiration (E) (Tyree & Zimmermann, 2013). Dry and hot conditions place greater tension, and therefore elevated stress on this liquid continuum, increasing the probability that microscopic bubbles are pulled through cell membranes and into the water transport column, nucleating cavitation (Sperry & Tyree, 1988; Cochard *et al.*, 1992). Current theory suggests that cavitation and the resulting air embolisms block the xylem, severing water transport from roots to leaves, killing downstream tissues by desiccation (Tyree, 1989). This hydraulic theory has revolutionized our understanding of why and when water-stress kills plants (McDowell *et al.*, 2008; Choat *et al.*, 2018; Brodribb *et al.*, 2020), yet widespread acceptance of hydraulic theory by biologists and modelers (Anderegg *et al.*, 2015; Sperry & Love, 2015; Sperry *et al.*, 2016; Wolf *et al.*, 2016; Eller *et al.*, 2020; Sabot *et al.*, 2020) has occurred in the absence of foundational evidence explicitly connecting hydraulic failure with tissue damage and death. This fundamental gap in understanding arises because of a lack of tools for high resolution temporal and spatial imaging of either cavitation or cell damage *in situ*. Thus, the aim of this study was to provide unequivocal evidence linking xylem

cavitation in leaf veins with downstream tissue damage using novel imaging methods on intact plants. Leaves provide the ideal organ to search for cavitation-induced tissue damage because they are the primary source of evaporative stress in the plant, and the organs most exposed to atmospheric perturbation, dehydration and damage by cavitation (Tyree & Ewers, 1991; Nardini *et al.*, 2001). In addition, the susceptibility and failure of leaf vascular networks under high evaporative load provide useful parallels with other supply networks including information and power distribution (Albert *et al.*, 2004; Witthaut *et al.*, 2016; Gavrilchenko & Katifori, 2019).

Here we developed a novel combination of technologies to track cavitation and its effects at high temporal and spatial resolution within leaves. To address the spatial challenge, we employed simultaneous *in situ* mapping of cavitation and tissue damage in the leaf using optical and fluorescence imaging to compare patterns of vascular and photosynthetic damage during leaf dehydration. Attributing cause based on a sequence of xylem cavitation followed by tissue damage is complicated by the fact that vascular plants are universally equipped with pores on leaves called stomata that close during dehydration. The resultant reduction in transpiration to a low residual value has the effect of disconnecting the timing of cavitation with its theoretical impact on the fatal dehydration of downstream tissue. To remove this time delay we created tomato (*Solanum lycopersicum* L.) double mutant plants (crossing *sit* and *flacca* mutants) that were unable to close stomata in response to dehydration due to multiple lesions in the biosynthetic pathway of the stomata-closing hormone abscisic acid (ABA). These mutant plants gave us a unique opportunity to precisely test the connections between transpiration, cavitation and cell damage in leaves.

Materials and Methods

Plant material

The *sitiens-flacca* (*sit flc*) double mutant was created at the University of Tasmania by crossing the homozygous, single gene mutants *sitiens* and *flacca* plants on the background *Solanum lycopersicum* L. c.v. ‘Rhinelands Rhune’. The resulting F1 progeny phenotypically resembled the wild type. The F1 plants were allowed to self and the resulting F2 progeny was genotyped to identify homozygous double mutant plants. Plants carrying the *flacca* allele were identified by PCR amplification of genomic DNA using primers specific to the wild type and *flacca* alleles (Sagi *et al.*, 2002) (See Extended Data Table 1), these primer sets resulted in products of different sizes. The *sitiens* allele was identified by a Cleaved Amplified Polymorphic Sequences marker; genomic DNA was amplified using gene specific primers (Extended Data Table 1) and the PCR product incubated with the restriction enzyme Bs1I (New England Biolabs), this enzyme specifically cleaved the wild type allele. Plants that were genotyped as homozygous for both mutant alleles were grown and seed collected for the following experiments.

Plants were germinated in the glasshouse facilities at the University of Tasmania in 1L pots with a potting mix medium comprising 7: 4 mix of composted fine pine bark and coarse washed river sand with fertilizer added Scott's Osmocote Classic 14-14-14 fertiliser (Scotts-Sierra, Marysville)). Plants were watered daily to full soil capacity and maintained at 21°C : 18°C, day : night temperatures, under natural light and daytime humidity of >60%, with sodium vapour lamps (PPFD = approx. 200 µmol quanta m^{-2} s^{-1}) used to extend the photoperiod to a constant 18 hours

Plants were grown between 2019 and 2020 and used for the following experiments when they were between 3 and five months old, at a height of 50-70cm.

ABA and stomatal response to leaf water potential

The ability of *sit flc* double mutant plants to produce ABA was examined in five plants each of the double mutant and Rhinelands Rhune background WT. Plants were measured first under well hydrated conditions and then they remained unwatered to reach lower values of leaf water potential over a period of 2-5 days. Each plant was sampled 2-3 times over the dehydration process. Plants that were not measured the same day were kept under the glasshouse conditions. Prior to measurement, plants were placed in a growth chamber for 20 minutes with light conditions of providing 500-800 µmol quanta m^{-2} s^{-1} photosynthetic photon flux density at the leaf surface, a temperature of 25°C and VPD of 2.0 kPa.

After this time, the sequence of measurements, with the minimum time possible between steps, was as follows: first, we took samples for ABA quantification; second, we took a leaflet from the same leaf for measuring leaf water potential with a Scholander pressure chamber (Soilmoisture Equipment Corp., Goleta, CA, USA); and third, we measured stomatal conductance with a gas exchange apparatus (LiCor 6800, Lincoln, NE, USA) in three leaflets neighbouring the leaflet sampled for ABA. Cuvette conditions were set to match the growth chamber conditions. On some occasions, it was not possible to measure leaf water potential with a pressure chamber (e.g. highly dehydrated leaves where tissue damage or cavitation violate the assumptions of the technique), so a leaf disc was taken with a 6-mm leaf punch and measured with a psychrometer (ICT Stem Psychrometer, Sydney Australia). For ABA samples, we used a 6-mm leaf punch to take five leaf discs per leaflet, we put them quickly into a 50 mL falcon tube (previously tared) and obtained the fresh weight with a precision balance. Immediately, these samples were covered with cold (-20 °C) 80% methanol in water with added BHT. Foliar ABA level was extracted, purified, and physicochemically quantified by the high precision method of ultra-performance liquid chromatography tandem mass spectrometry with an added internal standard according to the method of McAdam (McAdam, 2015).

Leaf xylem vulnerability to cavitation

The vulnerability of leaf xylem network to cavitation during dehydration was examined in four leaves from different plants. Whole plants were removed from pots and soil carefully washed from the roots. Plants were brought to the laboratory and arranged such that one leaf was fixed under the lens of a Leica M80 microscope where it was monitored for xylem cavitation in the leaf veins using the optical method (Brodribb *et al.*, 2016). This technique has the advantage of being non-invasive, allowing cavitation to be monitored in real time during dehydration. Although the technique does not directly measure changes in hydraulic conductance, it has been shown to accurately visualize xylem cavitation events (Johnson *et al.*, 2020) and if used correctly produces results that are highly comparable with flow methods (Gauthey *et al.*, 2020). Briefly, transmitted light images of intact leaves were captured as the plant dehydrated under laboratory conditions (22°C and 40-50% RH). Cavitation events can be visualized in the leaf venation by the rapid phase change from liquid water to water vapor inside the xylem conduits, which manifests as a detectable change in light transmittance through the leaf vein resulting from the differences in the refractive indices of water and air. Images of the whole leaf were captured every 3 minutes, and subsequent images were subtracted from each other to visualize rapid changes in light caused by cavitation. Using this method of image processing in ImageJ (https://imagej.nih.gov) it was possible to detect the cumulative area of pixels cavitated through time (see www.opensourceov.org for full details of this method). During dehydration, water potential was monitored using the proxy of collecting 6mm leaf discs from adjacent leaves (exposed to identical laboratory conditions) every 10 minutes and measuring their water potential in ICT stem psychrometers (ICT Sydney, Australia). Plants were monitored from their initial state of full hydration, then dehydrated until no further cavitation was recorded in the leaves (approximately 8 hours). Plots of water potential and cavitated area through time were combined to produce vulnerability curves showing %area of cavitated xylem as a function of water potential.

Whole plant evaporative damage

The susceptibility of *sitflc* leaves to water deficit caused by high transpiration was tested in whole plants. A total of 40 plants were propagated as described above in 2 L pots and measurements were performed from 6th May to 29th June 2020 when plants were 3 months of age.

On the afternoon of the day before measurements plants were moved into the laboratory, watered and covered with a dark plastic bag to ensure the plant was fully hydrated and dark adapted prior to the evaporation treatment. Dark adapting the plant allowed determination of photosynthetic damage using chlorophyll fluorescence, in particular the ratio of steady state and maximum chlorophyll fluorescence after application of a saturating flash of actinic light (Fv/Fm). Early in the morning of the following day, the plastic bag was removed and the distal region of each terminal leaflet (~ 4 cm^2) was clamped into an IMAGING-PAM (Walz, Effeltrich,

Germany) and exposed to a saturating flash to determine the spatial distribution of Fv/Fm across the leaf tissue, thus providing a control measure of chlorophyll fluorescence prior to treatment. This method was used because the imaging system provides spatially explicit values of Fv/Fm. Plants were covered again with the dark plastic bag and transported to a well-ventilated air-conditioned room regulated at constant temperature and constant relative humidity with light provided by banks of fluorescent and incandescent bulbs (providing 500-800 µmol quanta m^{-2} s^{-1} photosynthetic photon flux density). Water-saturated pots were covered in aluminium foil to prevent water evaporation from the soil and placed on a balance (0.01g) with three fine-wire thermocouples attached to leaves. Changes in mass (due to transpiration), leaf temperature, air temperature and humidity (HMP50; Vaisala, Vantaa, Finland) were logged on a CR10X datalogger (Campbell Scientific, Logan, UT, USA) every 60s over a period of 2 hours. Each plant was exposed to a different evaporative gradient ranging from 1.0 kPa leaf to air vapour pressure difference (VPD) to a maximum of 6.5 kPa. The VPD was regulated by changing the air temperature which ranged from 18.5ºC and 39.7ºC (the upper thermal damage threshold for *sit flc* mutant was >40°C- see main text). After 2 hours *E* was typically at steady state, at which point plants were returned to the laboratory and covered again with a plastic bag. The following day, after 14hours of dark adaptation, leaflets were detached from the plant and re-imaged with the IMAGING-PAM in order to visualize the extent of damage to the photosynthetic tissue, after which total leaf area was determined using a flatbed scanner.

The area of damaged photosynthetic tissue on each leaf was measured on the basis that photosynthetic damage was irreversible when Fv/Fm fell below 0.4 (Johnson *et al.*, 2020). By setting this threshold, it was possible to analyse all leaf fluorescence images (Image J) and calculate the percentage damage per leaflet. Average Fv/Fm was also measured to describe the degree of photosynthetic damage. The average damage per leaf each plant incurred during the VPD treatment was calculated from measurements of the terminal leaflet at each node. Individual leaflet damage was expressed as the final % damaged area minus the pre-treatment % damaged area.

Temperature threshold for photosynthetic damage

To ensure that leaf damage under evaporative stress was caused by dehydration and not temperature damage it was necessary to determine the thermal threshold for leaf damage in *sitflc* plants. This was done by exposing hydrated, excised, non-evaporating leaves to a range of heat treatments. Six well-watered, healthy plants were covered and dark-adapted with a wet plastic bag overnight. Leaflets were excised in the dark and imaged with the IMAGING-PAM to measure the dark-adapted state of photosynthetic tissue as indicated by Fv/Fm. Leaflets were sealed in a double plastic zip bag saturated with water vapour and immersed in a water bath constant temperature for 3 minutes (long enough to ensure temperature equilibration but not so long as to incur significant respiratory carbon or oxygen deficit. Temperature treatments were set at 5° steps between 25°C to 60°C with each leaf exposed to one temperature and between six and ten replicates per temperature. After 3

minutes leaflets were removed from the plastic bags in the dark and imaged again for Fv/Fm with the IMAGING-PAM to obtain final damage. Given that leaflets were prevented from transpiration, all the photosynthetic damage was exclusively related to thermal injury.

Leaf and whole-plant hydraulic conductance

Hydraulic conductances of leaves (K_{leaf}) and whole plants (K_{plant}) were measured to determine how tissue hydration was expected to change as a function of transpiration rate (E) during evaporative treatments. Whole plant hydraulic conductance was determined by applying Darcy's law (considering the plant as a porous medium) with a knowledge of the transpiration rate (E - mmol m^{-2} s^{-1}) and the pressure gradient across the whole plant ($\Delta\Psi$) (equation 1), and assuming steady-state conditions existed such that liquid flow through the plant was the same as the vapor flow out of the leaves.

(1) $K_{plant} = \frac{E}{\Delta\varphi}$

Five plants between three and four months of age were individually taken from the glasshouse, their pot surface covered with foil to prevent evaporation, and placed on a balance in a growth chamber set to 20°C and 50% humidity. Illumination was set at 300 µmol quanta m^{-2} s^{-1} at the leaf surface provided by a combination of fluorescent and incandescent lights. These mild evaporative conditions did not cause leaf wilting and were considered to represent the maximum K for the whole plant. After 3 hours equilibration a steady-state E was recorded, and leaf discs punched from three leaves in the canopy to determine leaf water potential (Ψ_{leaf}). Leaf discs were placed in an insulated psychrometer (Merrill, Logan, UT, USA) and allowed to equilibrate for three hours before a reading of leaf water potential was made. K_{plant} was calculated using equation (1) assuming that soil water potential was equal to 0 (as plants were well irrigated) and hence that $\Delta\Psi = \Psi_{leaf.}$ Plants were then harvested and measured on a flatbed scanner to determine leaf area. K_{plant} was normalized to water viscosity at 20°C.

Leaf hydraulic conductance (K_{leaf}) was similarly measured using the evaporative technique. Two leaves each from five plants were individually removed underwater in the morning and connected to a flowmeter to measure the flow rate of water into the leaf during an evaporational steady state. The flowmeter was constructed as a potential divider, measuring the pressure drop (equivalent to voltage) with a pressure transducer connected to a datalogger (Campbell Scientific, Logan, UT, USA) across a capillary of known conductance (Melcher *et al.*, 2012). Leaves were illuminated at a photosynthetic photon flux density of 500 µmol quanta m-2 s-1 and exposed to a range of leaf temperatures (one temperature per leaf) from 22-35°C (measured with a thermocouple in contact with the leaf). After connection to the flowmeter, leaves were allowed to come to an evaporative steady-state over 20 minutes. Leaves were then removed from the flowmeter, wrapped in a moist

paper towel and leaf water potential (Ψ_{leaf}) was measured using a Scholander pressure chamber Soilmoisture Equipment Corp., Goleta, CA, USA). Leaf hydraulic conductance (K_{leaf}) was calculated as Flow/ Ψ_{leaf} and normalized to leaf area and viscosity of 20°C (Fig.S2a, see later). A test of K_{leaf} sensitivity to water potential was made by fitting a linear regression to the plot of K_{leaf} *vs.* $\Psi_{leaf.}$ (Fig.S2b, see later).

Parallel monitoring of cavitation, gas exchange and PSII damage

To study the effects of high VPD on cavitation and photosynthetic tissue damage we employed a modified version of the optical vulnerability method (described above) for detecting cavitation in leaves.. We employed this method in combination with a gas exchange system that allowed us to view the leaf and record sequential transmitted light images, but also monitor gas-exchange and chlorophyll fluorescence in real-time.

Intact plants were left unwatered for 24 hours to bring the soil water potential into the range -0.5 to -0.7MPa. This initial soil drought enabled single leaf water potential to be lowered to the point of cavitation without exceeding the lethal leaf temperature of 40°C. Plants were brought to the lab and a single fully expanded terminal leaflet was placed into the cuvette of a Walz GFS-3000 gas exchange system equipped with a clear glass chamber top and bottom (Walz, Effeltrich, Germany) enabling leaves to be imaged under the microscope while simultaneously measuring gas exchange. Leaves were initially equilibrated to low vapor pressure deficit (VPD) conditions: leaf temperature = 25˚C, flow rate = 800 µmol s^{-1} water vapor = 20000ppm, resulting in a VPD of ~1 to 1.5 kPa. Leaves were dark adapted for 15 minutes and then a baseline fluorescence image (Fv/Fm) was captured using a Walz MINI-PAM imaging fluorimeter (Walz, Effeltrich, Germany) attached to the upper window of the gas exchange cuvette. Following imaging the fluorometer was removed and the cuvette was positioned within the field of view of an M80 stereo microscope (Leica, Wetzlar, Germany) and illuminated from below with a fiber optic light that supplied ~150 µmol m^{-2} s^{-1} photosynthetic photon flux density. The leaf was simultaneously imaged with a digital camera (Leica DMC4500) with fixed light and exposure settings set to capture transmitted light images of the leaf every 10 seconds for the duration of the experiment, allowing cavitation to be monitored in real time.

Leaves were initially equilibrated under the low VPD conditions until transpiration (E) and VPD reached a steady state after 30 minutes. Cuvette conditions were then set to increase VPD to a range between 3.0 and 6.0 kPa by decreasing the relative humidity in the chamber and increasing leaf temperature to 32-37˚ C. Supplemental heating was provided by an external heat source directed at the cuvette (Variable Temperature Heat Gun, Makita USA, La Mirada, California).

Leaves were maintained in the high VPD condition for at least 30 minutes or until cavitation was observed by viewing the sequential images from the stereo microscope. During this time the transmitted light images were

monitored for cavitation events which are detected by a change in grayscale color value in the midvein of the leaf between sequential images. In leaves with obvious cavitation, the leaf in the cuvette was immediately returned to the low VPD condition for a minimum of 15 minutes to observe recovery in leaf width and grayscale intensity. In leaves that did not exhibit cavitation during the high VPD exposure, the cuvette was returned to the low VPD conditions and the leaf monitored for recovery. Throughout the experiment the gas-exchange system allowed transpiration, stomatal conductance, VPD, and photosynthetic rate to be monitored.

At the end of each experiment the fiber optic light was turned off to allow the leaf to dark-adapt for 30 minutes before a second Fv/Fm image was captured to determine the degree of damage to the photosynthetic apparatus resulting from the VPD treatment and cavitation. A third Fv/Fm image was obtained from each leaf when possible between 24-48 hours after the end of the experiment. When leaves had significant cavitation, cavitated regions dried quickly and became brittle, and were difficult to measure for fluorescence.

Each image sequence was processed following the methods of Brodribb et al. (Brodribb *et al.*, 2016) to produce a sequence of ‘difference images’, where subsequent images in the original sequence are subtracted, such that the resulting difference image reveals changes only in the functional status of the leaf veins resulting from cavitation events. All image processing was performed using the open-source Fiji (ImageJ) software package and the OSOV plugin (http://www.opensourceov.org).

Regional leaf hydration proxies

Two proxies were used to determine the regional water potential distribution within leaves. Both leaf width and leaf light transmittance were expected to change due to changes in cell turgor as bulk leaf water potential changed. Both these candidate proxies could be measured at a regional scale within the leaf; hence it was necessary to confirm that each exhibited a reliable behaviour relative to bulk leaf water potential.

The relationship between leaf width and water potential was determined in 25 leaves allowed to dehydrate slowly while being scanned with a flatbed scanner set to an image resolution of 12600 pixels per inch (Fig.S4A, see later). Leaves were removed from 5 fully hydrated, bagged plants and immediately transferred to the scanner where an initial image was made of all leaves. Each leaf was fixed at the tip and base to the scan bed by adhesive tape allowing the margin to move in two dimensions during dehydration (preventing curling of the leaf margin). Following this, individual leaves were rescanned and removed from the scanner after different periods of dehydration, taking a leaf disc to determine their water potential at the last scan with a psychrometer. This procedure continued until leaf water potential reached -2MPa (where xylem cavitation and leaf damage was expected to occur). Shrinkage was calculated relative to the initial fully hydrated state in each leaf.

Changes in leaf light transmittance was used as an additional proxy for regional water potential variation within the leaf because it allowed neighboring regions within the leaf to be compared at a higher resolution than the leaf margin analysis (which integrated across the whole width of the leaf). To confirm a predictable relationship between Ψ_{leaf} and light transmittance, four leaves attached to whole plants were attached to the microscope, fixed along one edge in a similar way to those leaves clamped in the cuvette during gas-exchange and cavitation experiment described above. In this case however the whole plants were removed from the soil and allowed to dry slowly over approximately 4 hours until leaves were severely wilted and Ψ_{leaf} was close to -2MPa. During dehydration, leaf discs were punched from neighbouring leaves approximately every 20 minutes and transferred to a psychrometer (ICT) for measurement. Greyscale images were captured every 10 seconds during dehydration and the greyscale intensity measured (with Image J) at a location halfway between the midrib and margin. Greyscale intensity was plotted against Ψ_{leaf} (Fig.S4B, see later)

Regional leaf hydration during cavitation

The image sequences were also used to track the changes in two leaf parameters over time, leaf margin movement and grayscale color change. To track the movement of the leaf margin as the leaves rapidly lost water and shrank in width, six regions of interest (ROIs) were selected along the leaf margin using ImageJ/Fiji. The Manual Tracking plugin tool was used to record the x and y coordinates of the ROIs over time. For each leaf margin ROI we also selected a ROI reference point on the leaf mid vein and monitored the position of this ROI over time. Using a distance formula derived from the Pythagorean Theorem, we calculated the distance between the leaf margin ROI and the mid vein ROI. We then calculated the average decrease in leaf width over time for each sample.

Next, we selected six circular ROIs from the leaf surface with no major or minor veins to monitor the grayscale value over time. During the experiments obvious color changes occurred, and often with spatial and temporal coordination with the cavitation events. In the color image stacks these changes could be detected as a darkening of the leaf tissue, which was reversible in regions without cavitation, and permanent in regions close to cavitation events. Leaf color change was attributed to the loss of turgor and collapse of the palisade cells, which decreased the distance between cells, thereby decreasing the light transmittance and increasing absorptance. The similar effect was detectable in the grayscale images, and we monitored regions without veins to eliminate the influence of cavitation events from the grayscale changes. These ROIs were tracked over time to account for changes in grayscale value and movement of the leaf tissue due to desiccation.

RESULTS

Whole plant measurements

Levels of ABA in leaves of the *sitiens flacca* double mutant (*sit flc*) tomato plants were extremely low and insensitive to changes in leaf water deficit (Fig.S1a), eliminating any stomatal response to changes in humidity (measured here as the vapor pressure difference between the atmosphere and leaf; VPD), meaning that transpiration (E) from *sit flc* mutant plants increased proportionally with VPD (Fig.S1b). In well-watered plants, increasing E causes dehydration (a decline in leaf water potential- Ψ_{leaf}) due to friction in the water transport pathway from soil to leaves. Thus, by manipulating evaporative demand around a well-watered plant it was possible to induce very high rates of E, dehydrating leaves sufficiently to trigger damage. Following short exposure of 23 well-watered *sit flc* plants to a range of evaporative steady-states, a sharp increase in the percentage of leaf damage was observed in plants where E > 6 mmol m^{-2} s^{-1}, with damage exceeding 78% of total leaf area in leaves exposed to the maximum E of 13.8 mmol m^{-2} s^{-1} (Fig. 1).

To understand if damage to whole plants was related to xylem cavitation, we determined the vulnerability of leaf xylem to cavitation during dehydration (Supplemental Methods; Fig.2). The measured hydraulic conductance (K_{plant}) of whole plants normalized to 20°C was 2.8 ± 0.4 mmol m-2 s-1 MPa-1 (Fig.S2) which allowed the prediction (using Equation 2) of a damaging range of E based on the assumption that profound (95%) loss of xylem water transport function caused damage to leaves (Brodribb & Cochard, 2009).

Equation 2: $$\Psi_{leaf} = \frac{E}{K_{plant}}$$

The observed tissue damage resulting from exposure to high VPD in the *sit flc* mutant plants was consistent with the predicted pattern (Fig.1) assuming that high rates of transpiration leads to cavitation and blockage of the water transport system, causing subsequent desiccation and irreparable leaf tissue damage. However, the confirmation of this pathway as the causal agent in leaf damage requires precise spatial and temporal co-occurrence of cavitation and leaf damage.

Cavitation in individual leaves

Establishing an unambiguous connection between cavitation and leaf damage requires precise temporal and spatial resolution of the process of leaf damage. Thus, we tracked cavitation and tissue damage within single attached leaves of *sit flc* mutant plants where high rates of transpiration could be imposed upon individual leaves enclosed in a small gas exchange cuvette. Confining the evaporative load to a single leaf provided the greatest chance that cavitation would occur first in the tissue under observation and not in xylem tissue further upstream (in the stem or roots). Based on the mean measured hydraulic conductance of *sit flc* mutant leaves (13.2 ± 5.9 mmol m^{-2} s^{-1} MPa^{-1} at 20°C; n=18) and the range of Ψ_{leaf} shown to trigger leaf xylem cavitation

(Fig.2) it was predicted (using Equation 2) that leaf vein cavitation in well-watered plants would be initiated when E exceeded a transpiration rate of approximately 38 mmol m^{-2} s^{-1}. However, such high rates of transpiration could not be achieved in *sit flc* mutant leaves without exceeding the thermal damage limit of 40°C determined for photosynthetic electron transport in mutant leaves (Fig.S3). Thus, it was necessary to impose a small soil water deficit by withholding irrigation for 24 hours to induce a soil water potential range of -0.5 to -0.7 MPa thereby enabling cavitating water potentials to be reached by exposing leaves to VPDs between 3 and 6 kPa while maintaining leaf temperature < 40°C.

Ten *sit flc* leaves were enclosed in a transparent cuvette and exposed to VPD transitions which, in combination with mild soil water deficit, were predicted to cause leaf water potential (Ψ_{leaf}) to approach the vein cavitation threshold. When leaves were experimentally transitioned from a low to high VPD environment, E increased rapidly causing a decline in Ψ_{leaf}, seen as a dynamic reduction in both leaf width and leaf light transmittance as leaves shrank in size and became denser (Fig.3, Fig.S4). Two distinct trajectories were observed in leaves maintained at a Ψ_{leaf} close to the threshold of xylem cavitation. In the first scenario (60% of leaves) no cavitation was observed. When these uncavitated leaves were subsequently returned to the initial low VPD (1kPa) leaf volume recovered within 3 minutes, incurring no damage to the photosynthetic apparatus (Fig.S3a,b,c; Fig.S5 g,h,i,j). In the second scenario (40% of leaves) multiple large cavitation events were recorded in the leaf xylem network soon after transitioning to high VPD (Fig.3d,e,f). These cavitations always occurred in close succession, with multiple events initiating in the midrib and spreading into downstream arrays of connected minor veins in <10s (Fig. 3e). Immediately following cavitation, the rate of leaf shrinkage was observed to accelerate, indicating a rapid dehydration of the leaf mesophyll tissue downstream of the cavitation-damaged xylem (Fig. 3d; Video S1). Even though VPD was returned to low levels promptly following the observation of cavitation (within 3 minutes) no recovery in leaf volume was observed in leaves where cavitation had spread to all veins. Accompanying this rapid post-cavitation dehydration was a major loss of photosystem II fluorescence (dark adapted F_v/F_m) across the entire leaf lamina (Fig. 3f), indicating irreversible photosystem damage.

Within-leaf effects of cavitation

In two of the four leaves where cavitation was observed it was possible to arrest the spread of cavitation through the leaf vein network at an incipient stage by rapidly lowering VPD (within 1 minute of recording the first cavitation event), creating a regionally cavitated leaf. A common symptom of water stress attributed to local hydraulic failure is partial damage of leaf tips and margins (Cardoso *et al.*, 2020). These partially cavitated leaves provided a test of whether the observed regional spread of cavitation within single leaves of *sit flc* mutants could explain local tissue damage at the tips or margins of leaves. The patchy nature of early cavitation spread within these leaves created adjacent regions associated with cavitated and uncavitated

xylem. The rapid suppression of E after cavitation was predicted to allow only regions of leaf tissue supplied by uncavitated xylem to recover hydration, while tissue cut off from local vascular supply by cavitation was predicted to die. Immediately following cavitation in a region of the vein network, a sharp increase in the local rate of tissue dehydration occurred downstream (where roots are considered as the upstream source of water) of the recorded cavitation events, indicating a major disruption to the local water supply (Fig.4; Fig.S6; Video S2). Cavitation-induced blockage of the water transport system in these regions of the leaf was confirmed by a complete lack of recovery of mesophyll volume in tissues downstream of recorded cavitation when E was suppressed (Fig.4, Fig.S6, Extended Data Videos 2, 3). By contrast, neighboring non-cavitated regions of the leaf showed no inflection in the rate of change of leaf shrinkage, and recovered volume quickly upon restoration of the low VPD condition (similarly to uncavitated whole leaves), indicating that these regions maintained a sufficient hydraulic connection with the rest of the plant and soil.

Strongly localized damage to leaf photosynthetic apparatus was observed in mesophyll tissue immediately downstream of the observed leaf vein cavitation. In both leaves where partial cavitation occurred, we found that the photosynthetic quantum yield (F_v/F_m) of cells within the region supplied by the cavitated xylem network was very low (<0.4) within 30 minutes of returning leaves to the low VPD condition (Fig.4, Fig.S6). Fv/Fm values remained low 24h after the conclusion of the VPD treatments and these tissues became visibly necrotic (Fig.4), indicating that living tissues in this region were immediately and irreversibly damaged following cavitation. Neighbouring regions of the leaf unaffected by cavitation showed a minimal decline in quantum yield (F_v/F_m >0.7) once the leaf was returned to low VPD conditions and showed no difference in F_v/F_m from unstressed control *sit flc* leaves 24-48 h after the experiment. Damage to *sit flc* leaves was clearly defined by regions of minor vein cavitation and bounded by apparently functional larger veins (Fig 4, Fig.S6). This pattern is consistent with previous work (Brodribb *et al.*, 2016) showing that larger vein orders require a series of cavitations before losing function, while minor veins showed minimal redundancy. In all leaves where cavitation was recorded vein cavitation was precisely temporally matched to a steep increase in mesophyll dehydration rate presumably the ultimate agent of tissue damage (Fig.5).

Discussion

Our results unequivocally identify xylem cavitation as the causal element producing tissue death in the leaves of tomato mutant plants lacking the ability to regulate water loss from leaves. Leaf vein cavitation immediately compromised local water delivery to leaf mesophyll, leading to rapid downstream tissue dehydration, irreversible photosynthetic cell damage and ultimately tissue death. These observations provide the empirical support needed for justifying pervasive assumptions linking vascular failure and plant mortality during drought.

The *sit flc* mutant plants used here allowed manipulation of Ψ_{leaf} and rapid identification of cavitation-induced water supply disruption that would be impossible in plants with fully functional stomata. However, it is likely that an identical sequence of events occurs in plants subjected to acute drought stress in the field (Choat *et al.*, 2018). This is supported by the similarity in vein cavitation dynamics observed here compared with the patterns observed in non-mutant tomato leaves (Skelton *et al.*, 2017) and other species (Brodribb *et al.*, 2016). The only difference expected to occur in the leaves of wild plants would be that the progression from cavitation, to tissue damage, may take many hours in leaves with closed stomata as opposed to seconds in plants lacking stomatal control. Thus, the cavitation-induced severing of water supply is identified as the causal trigger for lethal tissue dehydration, although it may not be the only cause of damage in all species (Johnson *et al.*, 2018). What remains unknown is whether the final stage of xylem failure proceeds as a "runaway" feedback (Tyree & Sperry, 1988), or, as seems to be the case here, local leaf water transport fails at the point where cavitation spreads into the minor vein network (where a lack of xylem redundancy means that any cavitation is likely to sever the downstream local water supply). A minor-vein trigger for damage would explain why selection appears to favour the smallest rank of leaf veins being the most resistant to cavitation among the hierarchy of vein orders (Brodribb *et al.*, 2016; Scoffoni *et al.*, 2017), because cavitation of this rank of veins may never be recoverable. The reticulate venation patterning in tomato (as well as the majority of vascular plant species (Boyce & Knoll, 2002)) appears to allow containment of the spread of cavitation within the boundaries of the surrounding higher vein orders, allowing the recovery of tissue upstream of the cavitation events upon rewatering. Constraining the localized damage to smaller regions and preventing the systematic spread across the vein network highlights the importance of a reticulate network topology for providing redundancy and resiliency during partial network failure (Roth-Nebelsick *et al.*, 2001; Sack *et al.*, 2008; Corson, 2010).

Most recent modelling of drought-induced tree mortality assumes a threshold of xylem cavitation that triggers tree death (Anderegg *et al.*, 2015; Martin-StPaul *et al.*, 2017). These thresholds are defined based upon observational (Adams *et al.*, 2017) and experimental studies showing drought-induced mortality to be correlated with between 50% (Brodribb & Cochard, 2009) and 88% (Urli *et al.*, 2013) loss of water transport function due to cavitation. Although this mode of mortality is described as "hydraulic failure", it is clear this range of stem xylem damage is insufficient to cause accelerated tissue dehydration leading to organ death (Dietrich *et al.*, 2018). Assuming that the causal connection found here in tomato leaves between leaf cavitation and tissue death provides a general explanation for drought damage caused by hydraulic failure, then xylem thresholds for leaf death would be expected to be much closer to 100% damage to the xylem supply network upstream of the mesophyll tissue. Results here demonstrate that leaf rather than stem cavitation thresholds provide a causal measure of vulnerability to drought damage in tree crowns. However, extrapolating to whole-tree mortality may require more knowledge of how cavitation spreads between organs (Rodriguez-Dominguez *et al.*, 2018) and the dehydration sensitivity meristematic zones in the plant. For example, drought-induced

cavitation may cause leaves to be damaged and subsequently shed, but this defoliation may not be lethal in some tree species if stems and roots are less vulnerable to cavitation than leaves and can supply water to supply new growth following rainfall (Wolfe *et al.*, 2016; Skelton *et al.*, 2019) .

The ubiquitous observation that stomata in vascular plants close in response to reduced atmospheric humidity is classically explained in terms of efficiency of water use as the adaptive driver (Cowan, 1986). Whilst there is no doubt that stomatal closure achieves this end, the results here indicate that a primary adaptive advantage in stomatal closure is also the avoidance of cavitation and subsequent leaf damage at high evaporative demand. The inability of our well-watered ABA-deficient mutant tomato plants to close stomata in response to high evaporative demand was associated with dehydration-damage to a high proportion of leaves as the VPD increased. By linking this leaf damage to leaf xylem cavitation our data highlights the critical role played by ABA signaling, to close stomata and prevent cavitation in seed plants experiencing acute water deficit in either the soil or the atmosphere. These findings provide a solid foundation for ongoing work using plant hydraulic function, water balance and environmental change to predict crop and forest vulnerability to drought and climate change.

Acknowledgments: Authors acknowledge glasshouse staff (Michelle Lange and Tracy Winterbottom) for plant care. We thank Frances Sussmilch for designing the primers and CAPS marker and Shelly Urquhart for genotyping. **Funding:** This study was supported by funds from the Australian Research Council (DP190101552) to TB; a visiting research fellowship from UTAS to CB; Individual Fellowship from the European Union's Horizon 2020 research and innovation programme under the Marie Skłodowska-Curie grant agreement no. 751918-AgroPHYS to CMR-D. Authors declare no competing interests.

Author contributions: Conceptualization TB; Data Curation TB, CB, MC, CRD; Formal Analysis- TB, CB, MC; Funding Acquisition TB, CB, CRD; Investigation- TB, CB, MC, CRD, VT; Methodology- TB, CB; Project Administration TB; Resources, TB, CB, SM; Supervision- TB, CB; Visualization- TB, CB, MC; Writing (Original Draft)- TB, CB; Writing (review/editing)- TB, CB, MCC, CRD, SM;

References

Adams HD, Zeppel MJ, Anderegg WR, Hartmann H, Landhäusser SM, Tissue DT, Huxman TE, Hudson PJ, Franz TE, Allen CD. 2017. A multi-species synthesis of physiological mechanisms in drought-induced tree mortality. *Nature ecology & evolution* **1**(9): 1285.

Albert R, Albert I, Nakarado GL. 2004. Structural vulnerability of the North American power grid. *Physical review E* **69**(2): 025103.

Anderegg WR, Flint A, Huang C-y, Flint L, Berry JA, Davis FW, Sperry JS, Field CB. 2015. Tree mortality predicted from drought-induced vascular damage. *Nature Geoscience* **8**(5): 367.

Boyce CK, Knoll AH. 2002. Evolution of developmental potential and the multiple independent origins of leaves in Paleozoic vascular plants. *Paleobiology* **28**(1): 70-100.

Brodribb TJ, Bienaimé D, Marmottant P. 2016. Revealing catastrophic failure of leaf networks under stress. *Proceedings of the National Academy of Sciences* **113**(17): 4865-4869.

Brodribb TJ, Cochard H. 2009. Hydraulic Failure Defines the Recovery and Point of Death in Water-Stressed Conifers. *Plant Physiology* **149**(1): 575-584.

Brodribb TJ, Powers J, Cochard H, Choat B. 2020. Hanging by a thread? Forests and drought. *Science* **368**(6488): 261-266.

Cardoso AA, Batz TA, McAdam SA. 2020. Xylem embolism resistance determines leaf mortality during drought in Persea americana. *Plant Physiology* **182**(1): 547-554.

Choat B, Brodribb TJ, Brodersen CR, Duursma RA, López R, Medlyn BE. 2018. Triggers of tree mortality under drought. *Nature* **558**(7711): 531.

Cochard H, Cruiziat P, Tyree MT. 1992. Use of Positive Pressures to Establish Vulnerability Curves. *Further Support for the Air-Seeding Hypothesis and Implications for Pressure-Volume Analysis* **100**(1): 205-209.

Corson F. 2010. Fluctuations and Redundancy in Optimal Transport Networks. *Physical review letters* **104**(4): 048703.

Cowan IR 1986. Economics of carbon fixation in higher plants. In: Givnish TJ ed. *On the Economy of Plant Form and Function*. Cambridge: Cambridge University Press, 133-170.

Dietrich L, Hoch G, Kahmen A, Körner C. 2018. Losing half the conductive area hardly impacts the water status of mature trees. *Scientific Reports* **8**(1): 15006.

Eller CB, Rowland L, Mencuccini M, Rosas T, Williams K, Harper A, Medlyn BE, Wagner Y, Klein T, Teodoro GS, et al. 2020. Stomatal optimization based on xylem hydraulics (SOX) improves land surface model simulation of vegetation responses to climate. *New Phytologist* **226**(6): 1622-1637.

Gauthey A, Peters JM, Carins-Murphy MR, Rodriguez-Dominguez CM, Li X, Delzon S, King A, López R, Medlyn BE, Tissue DT. 2020. Visual and hydraulic techniques produce similar estimates of cavitation resistance in woody species. *New Phytologist* **228**(3): 884-897.

Gavrilchenko T, Katifori E. 2019. Resilience in hierarchical fluid flow networks. *Physical review E* **99**(1): 012321.

Johnson KM, Brodersen C, Carins-Murphy MR, Choat B, Brodribb TJ. 2020. Xylem embolism spreads by single-conduit events in three dry forest angiosperm stems. *Plant Physiology* **184**(1): 212-222.

Johnson KM, Jordan GJ, Brodribb TJ. 2018. Wheat leaves embolized by water stress do not recover function upon rewatering. *Plant, Cell & Environment*.

Martin-StPaul N, Delzon S, Cochard H. 2017. Plant resistance to drought depends on timely stomatal closure. *Ecology letters* **20**(11): 1437-1447.

McAdam SA. 2015. Physicochemical quantification of abscisic acid levels in plant tissues with an added internal standard by ultra-performance liquid chromatography. *Bio-protocol* **5**(18): 1-13.

McDowell N, Pockman WT, Allen CD, Breshears DD, Cobb N, Kolb T, Plaut J, Sperry J, West A, Williams DG. 2008. Mechanisms of plant survival and mortality during drought: why do some plants survive while others succumb to drought? *New Phytologist* **178**(4): 719-739.

Melcher PJ, Michele Holbrook N, Burns MJ, Zwieniecki MA, Cobb AR, Brodribb TJ, Choat B, Sack L. 2012. Measurements of stem xylem hydraulic conductivity in the laboratory and field. *Methods in Ecology and Evolution* **3**(4): 685-694.

Nardini A, Tyree MT, Salleo S. 2001. Xylem cavitation in the leaf of *Prunus laurocerasus* L. and its impact on leaf hydraulics. *Plant Physiology* **125**: 1700-1709.

Rodriguez-Dominguez CM, Carins Murphy MR, Lucani C, Brodribb TJ. 2018. Mapping xylem failure in disparate organs of whole plants reveals extreme resistance in olive roots. *New Phytologist* **218**(3): 1025-1035.

Roth-Nebelsick A, Uhl D, Mosbrugger V, Kerp H. 2001. Evolution and function of leaf architecture: a review. *Annals of botany* **87**: 533-566.

Sabot MEB, De Kauwe MG, Pitman AJ, Medlyn BE, Verhoef A, Ukkola AM, Abramowitz G. 2020. Plant profit maximization improves predictions of European forest responses to drought. *New Phytologist* **226**(6): 1638-1655.

Sack L, Dietrich EM, Streeter CM, Sánchez-Gómez D, Holbrook NM. 2008. Leaf palmate venation and vascular redundancy confer tolerance of hydraulic disruption. *Proceedings of the National Academy of Sciences* **105**(5): 1567-1572.

Sagi M, Scazzocchio C, Fluhr R. 2002. The absence of molybdenum cofactor sulfuration is the primary cause of the *flacca* phenotype in tomato plants. *The Plant Journal* **31**(3): 305-317.

Scoffoni C, Albuquerque C, Brodersen CR, Townes SV, John GP, Cochard H, Buckley TN, McElrone AJ, Sack L. 2017. Leaf vein xylem conduit diameter influences susceptibility to embolism and hydraulic decline. *New Phytologist* **213**(3): 1076-1092.

Skelton RP, Anderegg LDL, Papper P, Reich E, Dawson TE, Kling M, Thompson SE, Diaz J, Ackerly DD. 2019. No local adaptation in leaf or stem xylem vulnerability to embolism, but consistent vulnerability segmentation in a North American oak. *New Phytologist* **223**(3): 1296-1306.

Skelton RP, Brodribb TJ, Choat B. 2017. Casting light on xylem vulnerability in an herbaceous species reveals a lack of segmentation. *New Phytologist* **214**(2): 561-569.

Sperry JS, Love DM. 2015. What plant hydraulics can tell us about responses to climate-change droughts. *New Phytologist* **207**(1): 14-27.

Sperry JS, Tyree MT. 1988. Mechanism of water stress-induced xylem embolism. *Plant Physiology* **88**: 581-587.

Sperry JS, Wang Y, Wolfe BT, Mackay DS, Anderegg WR, McDowell NG, Pockman WT. 2016. Pragmatic hydraulic theory predicts stomatal responses to climatic water deficits. *New Phytologist* **212**(3): 577-589.

Tyree M 1989. Cavitation in trees and the hydraulic sufficiency of woody stems. *Annales des Sciences Forestières*: EDP Sciences. 330s-337s.

Tyree MT, Ewers FW. 1991. The hydraulic architecture of trees and other woody plants. *New Phytologist* **119**: 345-360.

Tyree MT, Sperry JS. 1988. Do woody plants operate near the point of catastrophic xylem dysfunction caused by dynamic water stress? *Plant Physiology* **88**: 574-580.

Tyree MT, Zimmermann MH. 2013. *Xylem structure and the ascent of sap*. Berling, Heidelberg, Germany: Springer Science & Business Media.

Urli M, Porté AJ, Cochard H, Guengant Y, Burlett R, Delzon S. 2013. Xylem embolism threshold for catastrophic hydraulic failure in angiosperm trees. *Tree physiology* **33**(7): 672-683.

Witthaut D, Rohden M, Zhang X, Hallerberg S, Timme M. 2016. Critical links and nonlocal rerouting in complex supply networks. *Physical review letters* **116**(13): 138701.

Wolf A, Anderegg WR, Pacala SW. 2016. Optimal stomatal behavior with competition for water and risk of hydraulic impairment. *Proceedings of the National Academy of Sciences* **113**(46): E7222-E7230.

Wolfe BT, Sperry JS, Kursar TA. 2016. Does leaf shedding protect stems from cavitation during seasonal droughts? A test of the hydraulic fuse hypothesis. *New Phytologist* **212**(4): 1007-1018.

Figure Legends

Figure 1. **Leaf damage in whole *sit flc* mutant plants provoked by 1 to 2 hours of exposure to a range of leaf to air vapor pressure difference (VPD)**. Leaf damage was determined from chlorophyll fluorescence (optimum quantum yield-F_v/F_m) imaged the day after treatment. **A).** Following a mild VPD exposure of 1.7 kPa most leaves remained undamaged, indicated by F_v/F_m images of terminal leaflets (left panels) where blue represents healthy tissue (F_v/F_m 0.7 to 0.8) and orange and red indicate damaged tissue (F_v/F_m < 0.4) and black indicates dead tissue. N refers to node. **B).** Following severe VPD treatment (5.3 kPa) most leaves exhibited damaged or dead tissue. **C)**. Mean leaf damage per plant (open circles = whole plant mean ± SD determined from one leaf per node; n = 15 to 20) increased as increasing VPD forced higher transpiration and leaf dehydration. Lethal xylem cavitation (>95% loss of hydraulic function) was predicted to occur at transpiration rates between 5.8 to 11.8 mmol m^{-2} s^{-1} (dotted vertical lines). This range of transpiration corresponded to a steep rise in leaf damage from 20% to 80%.

Figure 2. **Xylem vulnerability to cavitation in *sit flc* mutant leaves in response to dehydration (declining leaf water potential). A)** Each set of points represents an individual leaf from four separate plants, with the cumulative xylem area lost to cavitation summed across all vein orders. **B)**. Four images map the propagation of xylem embolism (false coloured according to the water potential at which the cavitation even appeared) in a single replicate leaf. The top image shows the raw image of the leaf at the initiation of drying.

Figure 3. **Cavitation in leaf veins during high transpiration causes a non-recoverable loss of leaf hydration and photosynthetic tissue damage in individual *sit flc* leaves. A)**. In a leaf where transpiration was not sufficiently high an increase in VPD (red trace with pink block indicating the duration of the the high VPD treatment) causes the leaf to shrink (blue trace) due to declining leaf water potential (a decline of 8% in width) but no cavitation was recorded.. Width then recovers rapidly upon return to low VPD at 7500s. Chlorophyll fluorescence (F_v/F_m) imaging in non-cavitated leaves shows a negligble change before **(B)** and after **(C)** VPD treatment. **D)**. In *sit flc* leaves where high VPD did casue cavitation (red circles, size indicating timing and vein order of cavitations), the leaf does not reach a new equilibrium width after the transition to high VPD_{leaf}, but instead it cavitates (pink circles) casuing the rate of leaf shrinkage to increases rapidly and not recover following return to low VPD. **E**) Shows the cumulative spatial distribution of cavitation (yellow) recorded in the leaf vein network. (F) Chlorophyll fluorescence images of the *sit flc* leaf following cavitation shows a

uniform reduction of F_v/F_m below 0.4, representing lethal damage to the photosynthetic apparatus. Bars = 5mm. See also Video S1

Figure 4. Temporal and spatial coordination of partial leaf xylem cavitation and associated damage to downstream photosynthetic cells within a single leaf. A) Local changes in leaf light transmittance (a proxy for local leaf hydration; see Fig.S4) in regions of the leaf upstream (blue line) and downstream (red line) of the xylem network affected by cavitation. The transition from low to high VPD (1.3 kPa to 3.7 kPa; pink shaded box) caused a parallel decline in leaf transmittance in both regions the leaf until cavitation events occurred in the mid vein and higher order veins (red circles, size is proportional to vein order), causing rapid dehydration (a decrease in leaf transmittance) of tissue cut off by cavitation. When returned to the low VPD condition (1.3 kPa), tissue upstream of the cavitation events recovered hydration, while downstream regions did not. Arrowheads with letters in (A) show the time points where the transmitted light and Fv/Fm images in (B) to (D) were captured. B) Transmitted light image of the same leaf in (A) before cavitation, showing the positions on the leaf used to calculate mean leaf transmittance in regions upstream (blue dots) and downstream (red dots) of the cavitation. C) Transmitted light image of the same leaf and the location of cavitation (yellow trace). D) Chlorophyll fluorescence (Fv/Fm) image of the leaf 30 minutes after returning to the low VPD state after cavitation indicates that damage was confined to the region downstream of cavitation. E) Chlorophyll fluorescence (Fv/Fm) image 24 hrs after the experiment showing damage and necrosis of tissue downstream of cavitation, but recovery of tissue upstream. Bars = 5mm. See also Video S2

Figure 5. **Leaf xylem cavitation immediately leads to a very rapid (and lethal) decline in leaf hydration as determined by both leaf shrinkage and leaf light transmission**. A 1:1 relationship was found between the timing of cavitation events detected in the mid vein and a significant increase in dehydration rate, determined by two proxies of leaf hydration; leaf width (blue points) or light transmission (grayscale value: red points) (n=5 leaves where cavitation was recorded). Red and blue shaded areas represent 95% confidence interval.

Supporting Information Legends

Fig. S1 Characterization of gas exchange and ABA production in the *sit flc* double mutant.

Fig. S2. Maximum whole plant hydraulic conductance of 5 *sit flc* plants calculated from steady state transpiration rate and leaf water potential.

Fig. S3. Susceptibility of *sit flc* leaves to tissue damage by high temperature.

Fig. S4. Two proxies used to indicate changes in the local hydration of sit flc leaves.

Fig. S5 Dynamic changes in the hydration of all measured single leaves subjected to step changes in VPD.

Fig. S6 Temporal and spatial coordination of leaf xylem cavitation in sit flc and damage to downstream photosynthetic cells.

Video S1. . Image sequence and corresponding plot of the leaf from Fig. 3

Video S2. Image sequence from the leaf in Fig 4

Video S3. Image sequence from the leaf in Fig S6

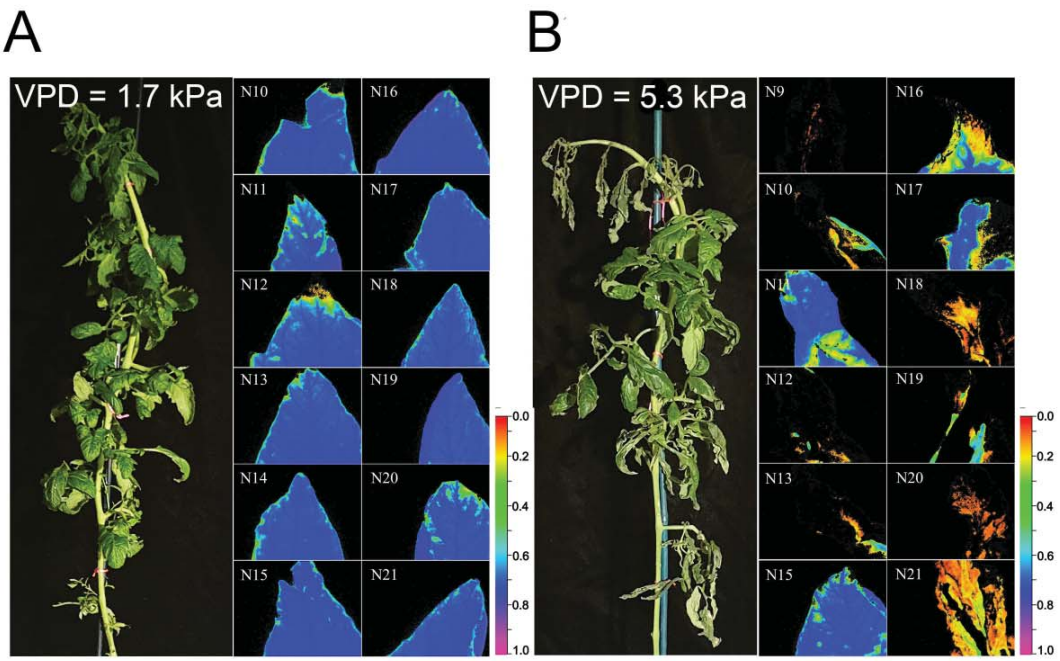

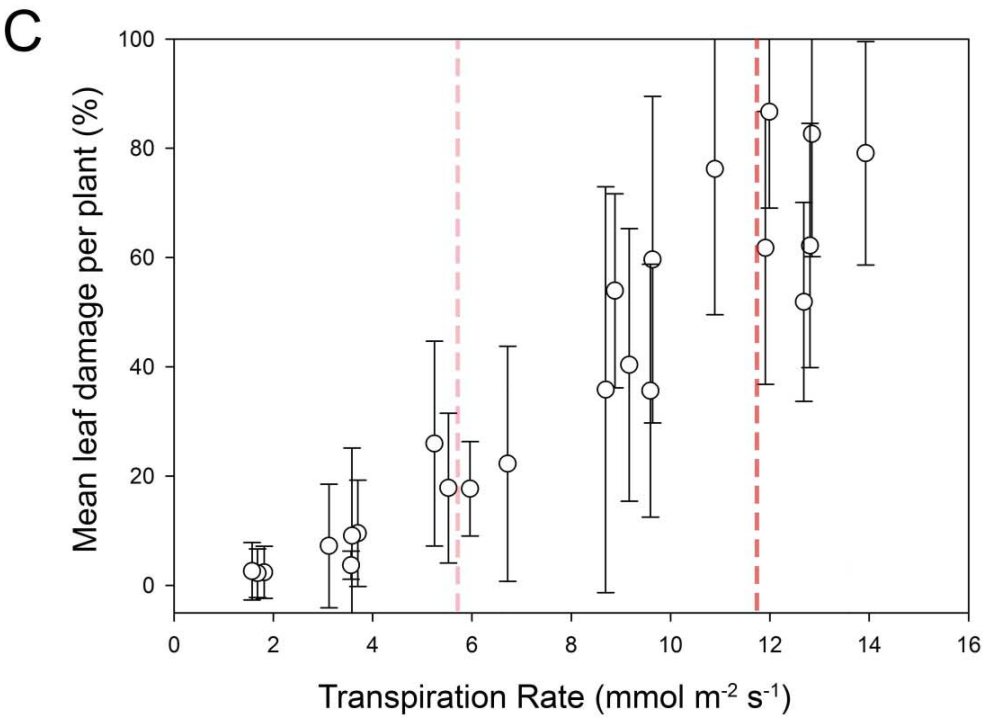

nph_17577_f1.jpg

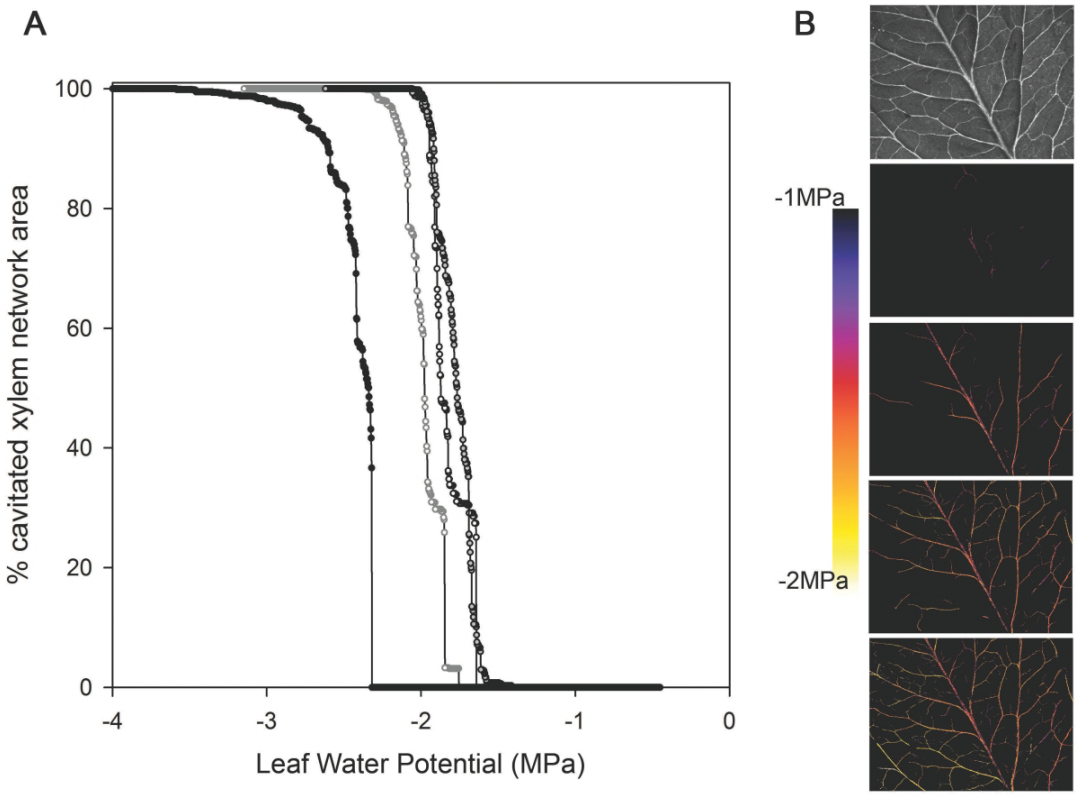

nph_17577_f2.jpg

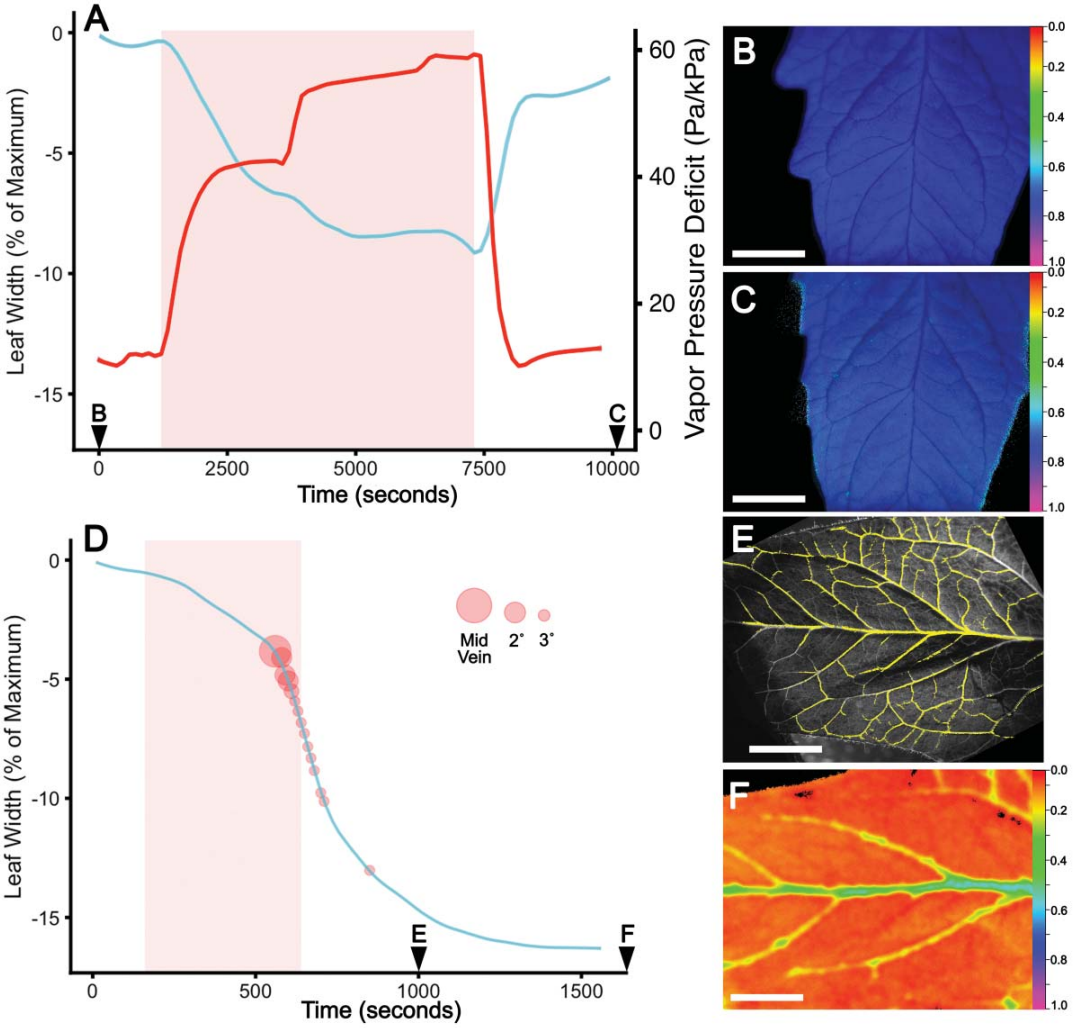

nph_17577_f3.tif

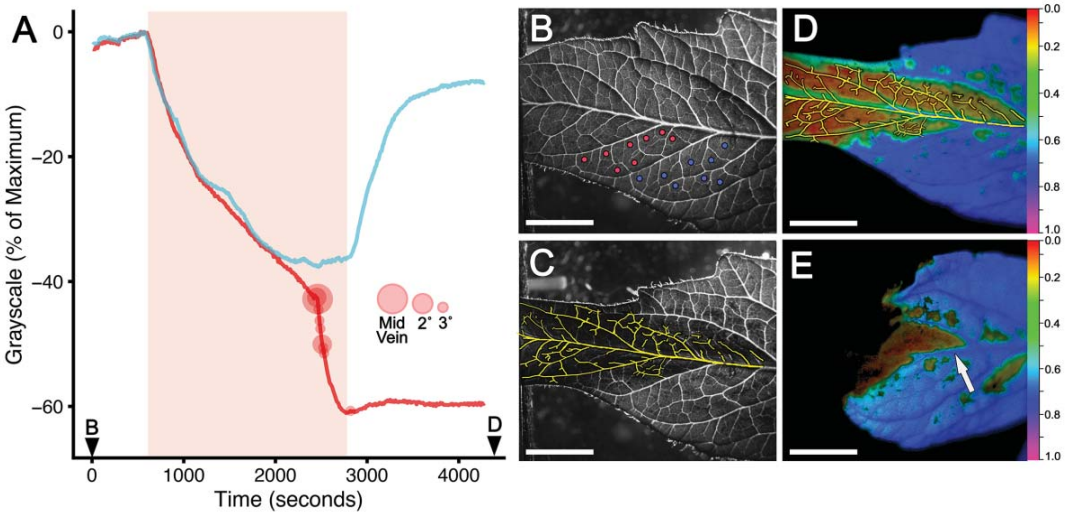

nph_17577_f4.tif

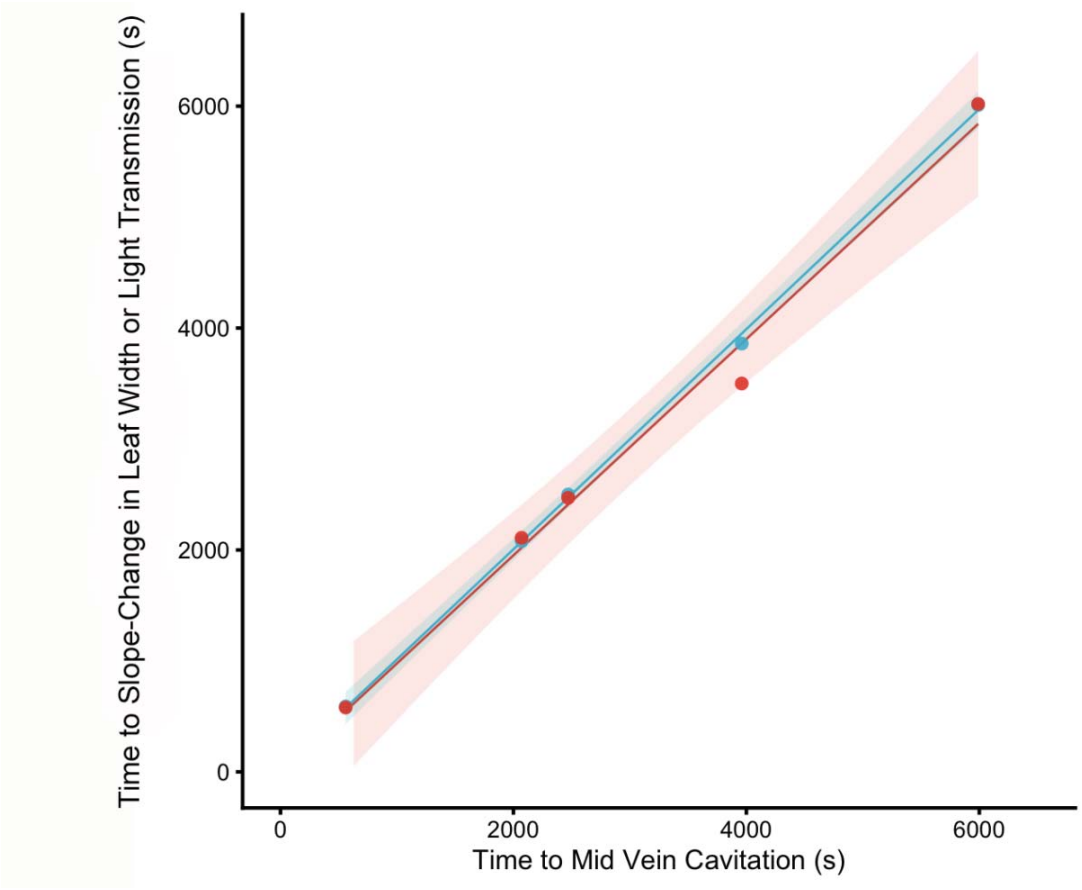

nph_17577_f5.tiff